frontiers in Chemistry

ORIGINAL RESEARCH
published: 09 December 2021
doi: 10.3389/fchem.2021.803464

Core-Shell-Like Structured Co_3O_4@SiO_2 Catalyst for Highly Efficient Catalytic Elimination of Ozone

Jingya Ding[1], Feng Cheng[2], Zhen Meng[1], Yan Cao[1], Fennv Han[1], Dongbin Chen[1], Mingxiang Cao[1], Guolin Zhang[3], Jiahao Kang[1], Shuxiang Xu[1] and Qi Xu[1]**

[1]School of Chemistry and Chemical Engineering, Yancheng Institute of Technology, Yancheng, China, [2]Key Laboratory for Advanced Technology in Environmental Protection of Jiangsu Province, Yancheng Institute of Technology, Yancheng, China, [3]School of Mechanical Engineering, Yancheng Institute of Technology, Yancheng, China

Co_3O_4 is an environmental catalyst that can effectively decompose ozone, but is strongly affected by water vapor. In this study, Co_3O_4@SiO_2 catalysts with a core-shell-like structure were synthesized following the hydrothermal method. At 60% relative humidity and a space velocity of 720,000 h^{-1}, the prepared Co_3O_4@SiO_2 obtained 95% ozone decomposition for 40 ppm ozone after 6 h, which far outperformed that of the 25wt% Co_3O_4/SiO_2 catalysts. The superiority of Co_3O_4@SiO_2 is ascribed to its core@shell structure, in which Co_3O_4 is wrapped inside the SiO_2 shell structure to avoid air exposure. This research provides important guidance for the high humidity resistance of catalysts for ozone decomposition.

Keywords: ozone decomposition, Co_3O_4, SiO_2, Core@Shell constructure, relative humidity 1. introduction

OPEN ACCESS

Edited by:
Lin Sun,
Yancheng Institute of Technology, China

Reviewed by:
Zetian Tao,
University of South China, China
Junjian Miao,
Shanghai Ocean University, China

****Correspondence:***
Feng Cheng
chf@ycit.edu.cn
Qi Xu
ycxqsteve@163.com

Specialty section:
This article was submitted to Nanoscience, a section of the journal Frontiers in Chemistry

Received: *28 October 2021*
Accepted: *17 November 2021*
Published: *09 December 2021*

Citation:
Ding J, Cheng F, Meng Z, Cao Y, Han F, Chen D, Cao M, Zhang G, Kang J, Xu S and Xu Q (2021) Core-Shell-Like Structured Co_3O_4@SiO_2 Catalyst for Highly Efficient Catalytic Elimination of Ozone. Front. Chem. 9:803464. doi: 10.3389/fchem.2021.803464

INTRODUCTION

Ozone is widely used in food, medicine, and waste treatment owing to its excellent oxidizing ability (Alameddine et al., 2021; Kim et al., 2022). However, even low concentrations of ozone are harmful to human health, especially to the eyes, nose, and throat (Ferrara et al., 2020; Ferrara et al., 2021). The maximum eight-hour average concentration of ozone allowed by the World Health Organization is 100 $\mu g/m^3$. Ozone concentrations in the atmosphere near ground level have considerably increased in recent years due to increased levels of volatile organic compounds and nitrogen oxides (Ou et al., 2016). Ozone in the outdoor air can infiltrate into indoor environments. Indoor ozone is considered more harmful than outdoor ozone because modern humans spend most of their time indoors (Abbass et al., 2017; Namdari et al., 2021; Nazaroff and Weschler 2021). The development of environmental technologies to effectively eliminate ozone is therefore necessary.

There are four common treatment methods to eliminate ozone: activated carbon (Yu et al., 2020); absorption (Yang et al., 2017); thermal decomposition and catalytic decomposition (Gopi et al., 2017; Ma et al., 2017; Gong et al., 2018). Catalytic decomposition is considered to be one of the most feasible and effective methods for ozone removal (Li et al., 2020). Noble metals and transitional metal oxides are common catalysts for heterogeneous reactions including decomposition of ozone (Nikolov et al., 2010; Gong et al., 2017; Deng et al., 2019; Tao et al., 2021a; Tao et al., 2021b). Among the transition metal oxides, Co_xO_y catalysts with higher oxidation states have exhibited higher ozone decomposition performance than other cobalt oxide catalysts (Tang et al., 2014a). Abdedayem (Abdedayem et al., 2017) demonstrated that the ozone decomposition abilities of Co_3O_4 support on loaded olivine is proportional to its dispersion degree. However, numerous metal oxide catalysts suffer from interactions with water vapor, and including cobalt oxides (Zhu et al., 2021). It is generally believed that water vapor affects ozone decomposition via competitive adsorption with the transition metal oxides on the active sites (Jia et al., 2016).

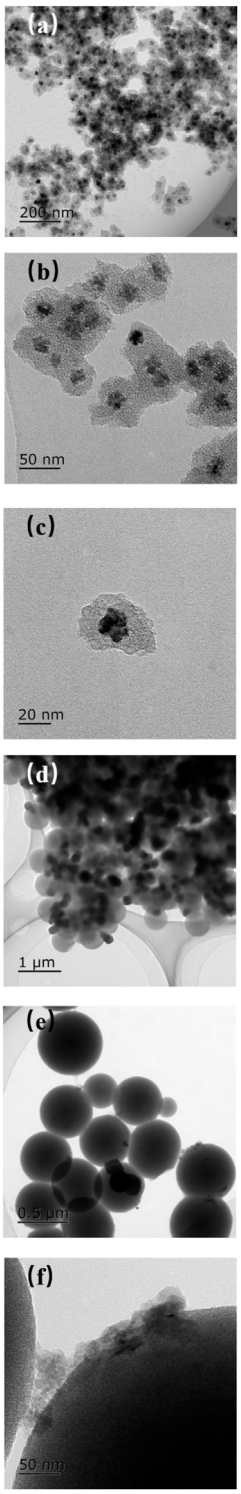

FIGURE 1 | Scanning electron microscope images of Co_3O_4@SiO_2 **(A–C)** and $25Co_3O_4/SiO_2$ **(D–F)**.

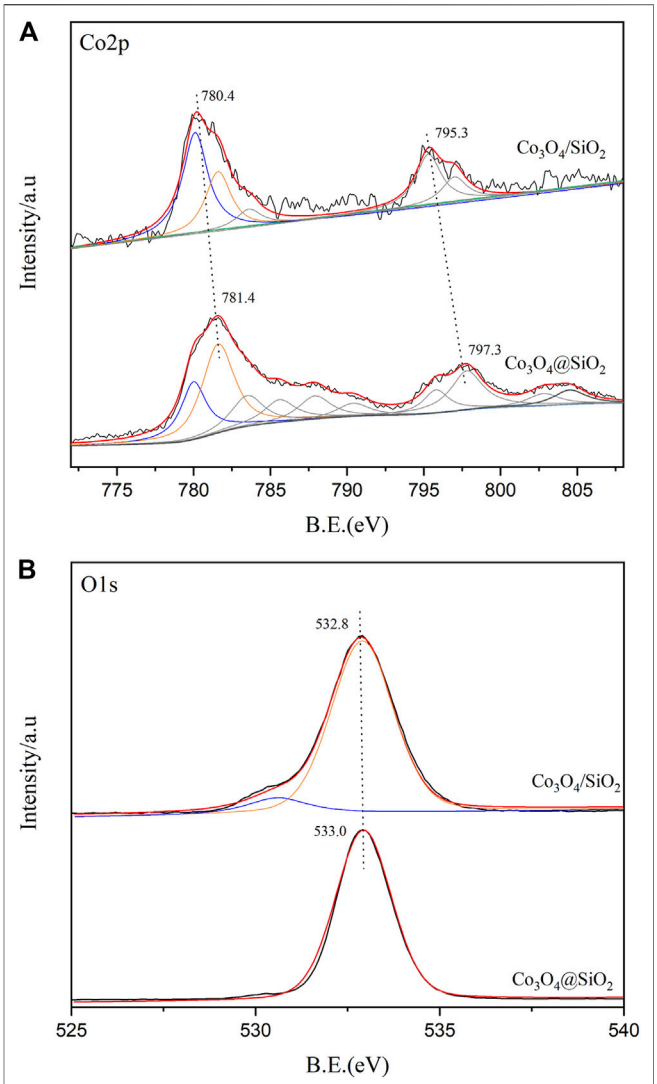

FIGURE 2 | XPS survey spectra of Co_3O_4@SiO_2 and $25Co_3O_4/SiO_2$.

In this study, core@shell structure catalysts were synthesized with mesoporous silica as the shell and Co_3O_4 nanoparticles as the core (Co_3O_4@SiO_2) following the solvothermal route using polyvinylpyrrolidone (PVP) as the capping agent. For comparison, spherical silica supported different additions of Co_3O_4 and labeled xCo_3O_4/SiO_2, where x = 10, 15, and 20, or 25%. The ozone decomposition performance of xCo_3O_4/SiO_2 increased with increasing Co_3O_4. The $25Co_3O_4/SiO_2$ and Co_3O_4@SiO_2 catalysts yielded high ozone decomposition activity at 20% relative humidity. The ozone elimination activity of $20Co_3O_4/SiO_2$ sharply decreased upon increasing the relative humidity to 60%, and the Co_3O_4@SiO_2 catalyst exhibited a better moisture resistance performance for ozone decomposition. This study provides important insights for the further development of coated catalysts for gaseous ozone decomposition.

EXPERIMENTAL METHODS

Catalyst Preparation

Co_3O_4@SiO_2 was synthesized in accordance with previously published studies (Khan et al., 2015). First, 0.70 g PVP and

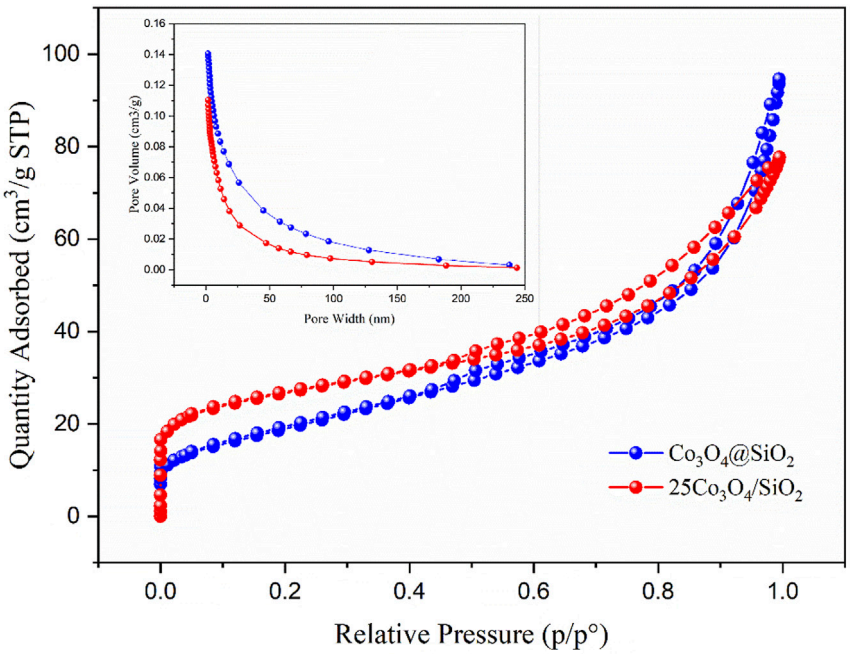

FIGURE 3 | Nitrogen adsorption-desorption isotherms and BJH pore-size distribution curves of Co_3O_4@SiO_2 and $25Co_3O_4/SiO_2$.

0.35 g $Co(NO_3)_2{\cdot}6H_2O$ were dissolved in 40 ml ethanol. The solutions were transferred to stainless steel lined with Poly tetra fluoroethylene (PTFE) in an autoclave and heated at 453 K for 4 h. The obtained black powder was dispersed in 103.8 ml ethanol, to which 82.8 ml distilled water, 7.2 ml 25% aqueous ammonia solution, 0.3 g cetyltrimethylammonium bromide, and 1.0 ml tetraethoxysilane were added. The solution was stirred for 48 h at room temperature. The product was collected via filtration, washed three times with distilled water, dried at 333 K, and then calcined at 773 K for 6 h. The finished samples were denoted as Co_3O_4@SiO_2 (wt% = 30%). SiO_2 was impregnated with 10, 15, 20, or 25% cobalt loading in an ethanol solution of cobalt nitrate, and the resulting product was calcined at 773 K for 6 h. The prepared samples were labeled as $10Co_3O_4/SiO_2$, $15Co_3O_4/SiO_2$, $20Co_3O_4/SiO_2$, and $25Co_3O_4/SiO_2$, respectively.

Catalyst Characterization

The samples were characterized by X-ray diffraction (XRD) using a D/max-RB diffractometer. X-ray photoelectron spectroscopy (XPS) was performed using a Thermo Fisher ESCALAB 250Xi. Morphological and microstructural characterizations were carried out using a Hitachi EM-3010 transmission electron microscope (TEM). The surface areas were calculated by the Brunauer-Emmett-Teller (BET) method. The pore diameters were estimated from the desorption branchers of the isotherms based on the Barrett-Joyner-Halenda (BJH) model.

Catalyst Test

The ozone decomposition activity of the prepared catalysts was evaluated using a flow-through quartz tube reactor (inner diameter = 10 mm) with 0.10 g of catalyst separated by quartz sand at different temperatures and relative humidity (20, 40, and 60%) under atmospheric pressure conditions. Ozone was generated by flowing 20% O_2/N_2 compressed gas through an ozone generator. The relative humidity of the gas stream was measured using a humidity probe (Benetech, GM1361+). The total gas flow rate passing through the quartz reactor was controlled at 1,500 ml/min and contained 40 ppm O_3. The ozone concentrations at the inlet and outlet were detected using a 106-L ozone online analyzer (2B Technologies, Boulder, Co, United States). The ozone conversion was calculated according to:

$$\text{Ozone conversion} = \frac{C_i(O_3) - C_o(O_3)}{C_i(O_3)} \times 100\%$$

where $c_i(O_3)$ and $c_o(O_3)$ represent the inlet and outlet ozone concentrations, respectively.

RESULTS AND DISCUSSION

Catalyst Characteristics

The morphology and nanostructure of the catalysts were observed by TEM. **Figure 1A–C** show that the Co_3O_4@SiO_2 nanoparticles were relatively dispersible with an average size of 40 nm. This indicates that PVP can prevent Co_3O_4 nanoparticle agglomeration under hydrothermal conditions. **Figure 1D–F** show that the spherical Co_3O_4/SiO_2 composites prepared via incipient wetness impregnation were highly dispersed with a relatively smooth external surface. This indicates that a

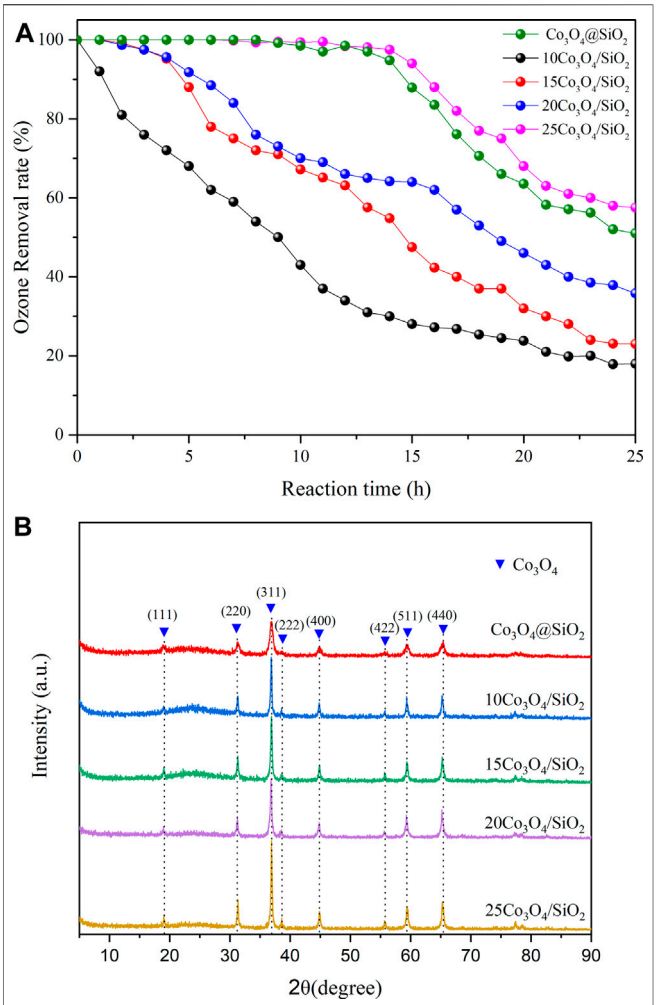

FIGURE 4 | (A) Ozone removal rates and **(B)** XRD patterns of Co_3O_4@SiO_2 and xCo_3O_4 (x = 10, 15, 20, and 25). Temperature = 25°C; relative humidity = 20%.

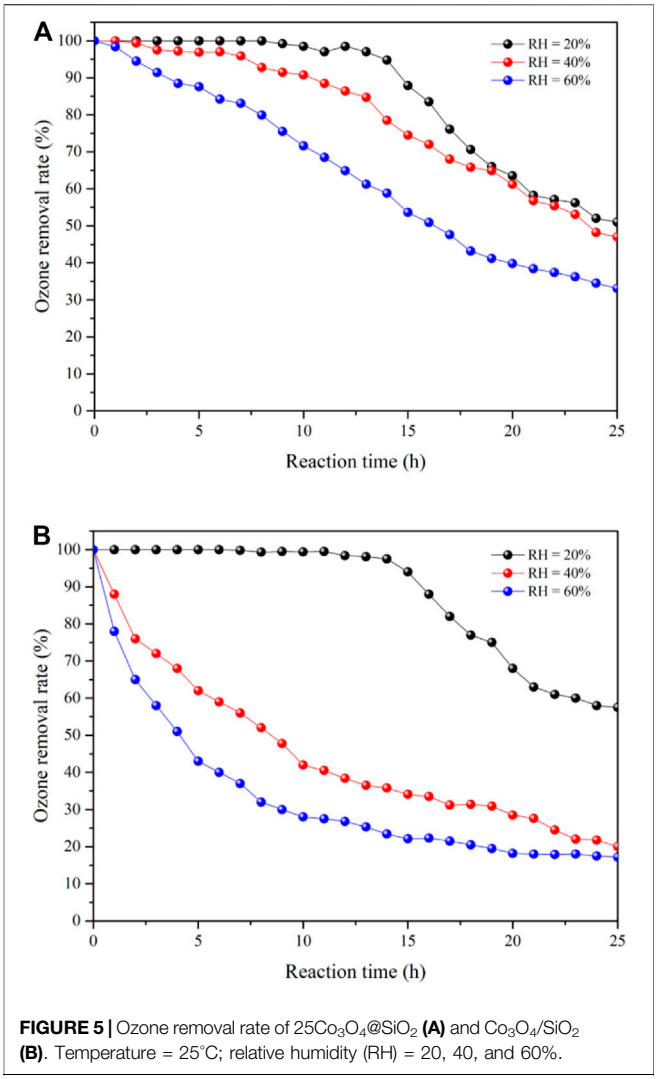

FIGURE 5 | Ozone removal rate of 25Co_3O_4@SiO_2 **(A)** and Co_3O_4/SiO_2 **(B)**. Temperature = 25°C; relative humidity (RH) = 20, 40, and 60%.

majority of the Co_3O_4 nanoparticles were incorporated into the mesopores (Xie et al., 2011). With regard to the spent Co_3O_4/SiO_2 catalyst, the large aggregates were clearly located on the external surface of the spherical SiO2 support, and indicating that small Co_3O_4 nanoparticles outside of the mesopores easily agglomerated into large Co_3O_4 aggregates during the reaction.

X-ray photoelectron spectroscopy (XPS) tests were performed to detect the chemical state and composition of the element catalyst surface. According to the previously reported Co_3O_4 spectrum (Gao et al., 2021), the Co 2p spectrum of Co_3O_4 (**Figure 2A**) consists of two peaks, Co $2p_{3/2}$ and Co $2p_{1/2}$, located at 779.9 and 794.8 eV, respectively. However, the Co $2p_{3/2}$ and Co $2p_{1/2}$ peaks in the Co_3O_4@SiO_2 and Co_3O_4/SiO_2 catalysts shifted to approximately 781.0 and 796.0 eV, respectively, both of which occur at higher energies than those of pure Co_3O_4. This shift is mainly due to the interaction between the silica and Co_3O_4 species, which results in a charge transfer from the Co_3O_4 to the SiO_2 support and has a positive impact on the cobalt catalytic performance.

The atomic surface contents of cobalt were 0.8 and 7.6% for the Co_3O_4@SiO_2 and Co_3O_4/SiO_2 catalysts, respectively. This significant difference further confirms that the preparation of Co_3O_4@SiO_2 successfully encapsulated Co_3O_4 into the SiO_2 matrix. The O 1 s spectra of the catalysts are shown in **Figure 2B**. The main O 1 s peak centered at 533.0 eV represents the lattice oxygen of Co_3O_4 and SiO_2, but is difficult to be accurately distinguished. The oxygen in the unreducible silica has no notable effect on the catalysis of ozone.

Figure 3 shows the nitrogen isothermal adsorption-desorption curves and pore size distributions of the Co_3O_4@SiO_2 and 25Co_3O_4/SiO_2 catalysts. The nitrogen adsorption-desorption isotherms clearly show that both samples have typical hysteresis loops and are classified as type-IV isotherms, thus indicating that the samples have a mesoporous structure. The average pore diameter of the two samples ranges between 6 and 9 nm. The pore volume of Co_3O_4@SiO_2 (0.15 cm^3/g) is larger than that of Co_3O_4/SiO_2 (0.11 cm^3/g). The specific surface area of Co_3O_4/SiO_2 is 94.8 m^2/g, which is 1.5 times greater than that of Co_3O_4@SiO_2 (68.8 m^2/g). The specific surface area of a catalyst is

generally believed to have a substantial impact on the catalytic activity, in which catalysts with larger specific surface areas usually have higher catalytic activities. Effect of Co_3O_4@SiO_2 and Co_3O_4/SiO_2 on ozone decomposition.

The ozone decomposition rates of Co_3O_4@SiO_2 and Co_3O_4/SiO_2 with different Co_3O_4 loadings were evaluated in a gas flow with 40 ppm ozone at 20% relative humidity. The activity of the $10Co_3O_4$/SiO_2 catalyst dropped sharply within 1 h, and the $15Co_3O_4$/SiO_2 and $20Co_3O_4$/SiO_2 catalysts dropped to 94% ozone conversion after 4 h. The time to achieve 100% ozone removal rate increased to 9 h for a Co_3O_4 load of 25%. However, the Co_3O_4@SiO_2 catalyst with 30 wt% loading achieved the same ozone removal rate as that of $25Co_3O_4$/SiO_2. This indicates that the ozone elimination rate is proportional to the Co_3O_4 catalyst load. The XRD patterns of the as-prepared catalysts are shown in **Figure 4B**, in which all of the obtained samples exhibit the same peaks, corresponding to pure Co_3O_4 (JCPDS No. 42-1,467) (Agilandeswari and Rubankumar 2016). This indicates that the crystalline phase is well maintained during the treatment. The diffraction peaks of both Co_3O_4@SiO_2 and xCo_3O_4/SiO_2 are sharp and intense, and the peak intensities gradually increase with increasing Co_3O_4 catalyst load. The $25Co_3O_4$/SiO_2 catalyst exhibits more intense peaks at 36.5 than Co_3O_4@SiO_2 for a similar Co_3O_4 content. This indicates that the Co_3O_4@SiO_2 core-shell structure weakens the intensity of the characteristic peaks, and that the Co_3O_4 crystalline material is well inside the mesoporous silica particles. Effect of $25Co_3O_4$@SiO_2 and Co_3O_4/SiO_2 on ozone decomposition under different relative humidity conditions.

Figure 5A,B show the ozone removal rates of $25Co_3O_4$@SiO_2 and Co_3O_4/SiO_2, respectively, at relative humidity conditions of 20, 40, and 60%. The $25Co_3O_4$@SiO_2 and Co_3O_4/SiO_2 catalysts exhibit similar ozone removal rates at 20% relative humidity. The $25Co_3O_4$/SiO_2 catalyst shows 99% ozone conversion for 11 h at 20% relative humidity. The removal rate then sharply drops and ultimately stabilizes at 60%. It is noted that the ozone removal rate sharply decreases with increasing relative humidity, especially when the relative humidity is increased from 40 to 60%. For Co_3O_4@SiO_2, the ozone removal rate begins to decrease during the first 12 h of the reaction runs with a gas flow of 40 ppm ozone, and then decreases to 60% when the reaction has been maintained for 24 h. The ozone removal rate of Co_3O_4@SiO_2 shows a different trend from that of $25Co_3O_4$/SiO_2 at 40% relative humidity. When the relative humidity is increased to 60%, the ozone removal rate sharply decreases and remains at 30%, which is approximately 10% higher than that of $25Co_3O_4$/SiO_2. This indicates that the main reason for the different performance of the two catalysts is their differing structures. The Co_3O_4 loaded on the surface of SiO_2 is directly exposed to the reaction environment. The accumulation of oxygen atoms and adsorption of water vapor thus lead to catalyst deactivation. In contrast, in the Co_3O_4@SiO_2 catalyst, the Co_3O_4 is wrapped by SiO_2, and which isolates water vapor and prevents it from directly contacting with the Co_3O_4. The deactivation can thus be attributed to the accumulation of oxygen atoms.

Proposed Mechanism

According to the experimental results, we proposed a possible mechanism involving oxygen vacancies (O_v) as depicted below. Initially, the ozone molecule is adsorbed on the oxygen vacancy of the surface of Co_3O_4 and the ozone decompose into oxygen, while another oxygen atom is left on the surface of Co_3O_4 and form lattice oxygen (O^{2-}). Subsequently, the ozone molecule reacts with lattice oxygen and form oxygen and O_2^{2-}. Finally, the O_2^{2-} breaks off the Co_3O_4 surface in form of oxygen.

$$O_3 + O_V \rightarrow O_2 + O^{2-} \quad (R1)$$
$$O_3 + O^{2-} \rightarrow O_2 + O_2^{2-} \quad (R2)$$
$$O_2^{2-} \rightarrow O_2 + O_v \quad (R3)$$

CONCLUSION

In this work, Co_3O_4@SiO_2 and xCo_3O_4/SiO_2 (x = 10, 15, 20, and 25) catalysts were successfully synthesized using the hydrothermal method. Under similar loading conditions, the ozone removal rates of Co_3O_4@SiO_2 and $25Co_3O_4$/SiO_2 were nearly the same under flow conditions of 40 ppm ozone and 20% relative humidity. When the relative humidity increased to 60%, the ozone removal rate of Co_3O_4@SiO_2 was higher than that of $25Co_3O_4$@SiO_2. XRD, XPS, and BET characterizations indicate that the high Co_3O_4@SiO_2 performance is related to the core@shell structure. This study thus provides insight for developing catalysts to effectively remove gaseous ozone.

DATA AVAILABILITY STATEMENT

The original contributions presented in the study are included in the article/**Supplementary Material**, further inquiries can be directed to the corresponding authors.

AUTHOR CONTRIBUTIONS

FC and QX conceived the idea. JD, YC, and FH designed and fabricated the sample, ZM, DC, MC, GZ, JK, and SX conducted the the expriment. All the authors contrubuted to analysis of the data and draft of the manuscript.

FUNDING

National Key Research and Development Program of China 2016YFC0209203 Funding for school-level research projects of Yancheng Institute of Technology xjr2019055.

SUPPLEMENTARY MATERIAL

The Supplementary Material for this article can be found online at: https://www.frontiersin.org/articles/10.3389/fchem.2021.803464/full#supplementary-material

REFERENCES

Abbass, O. A., Sailor, D. J., and Gall, E. T. (2017). Effectiveness of Indoor Plants for Passive Removal of Indoor Ozone. *Building Environ.* 119, 62–70. doi:10.1016/j.buildenv.2017.04.007

Abdedayem, A., Guiza, M., Rivas Toledo, F. J., and Ouederni, A. (2017). Ozone Decomposition over Cobalt Supported on Olive Stones Activated Carbon: Effect of Preparation Method on Catalyst Activity. *Ozone: Sci. Eng.* 39, 435–446. doi:10.1080/01919512.2017.1331729

Agilandeswari, K., and Rubankumar, A. (2016). Synthesis, Characterization, Optical, and Magnetic Properties of Co3O4 Nanoparticles by Quick Precipitation. *Synth. Reactivity Inorg. Metal-Organic, Nano-Metal Chem.* 46, 502–506. doi:10.1080/15533174.2014.988807

Alameddine, M., Siraki, A., Tonoyan, L., and Gamal El-Din, M. (2021). Treatment of a Mixture of Pharmaceuticals, Herbicides and Perfluorinated Compounds by Powdered Activated Carbon and Ozone: Synergy, Catalysis and Insights into Non-free OH Contingent Mechanisms. *Sci. Total Environ.* 777, 146138. doi:10.1016/j.scitotenv.2021.146138

Deng, H., Kang, S., Ma, J., Wang, L., Zhang, C., and He, H. (2019). Role of Structural Defects in MnOx Promoted by Ag Doping in the Catalytic Combustion of Volatile Organic Compounds and Ambient Decomposition of O3. *Environ. Sci. Technol.* 53, 10871–10879. doi:10.1021/acs.est.9b01822

Ferrara, F., Pambianchi, E., Pecorelli, A., Woodby, B., Messano, N., Therrien, J.-P., et al. (2020). Redox Regulation of Cutaneous Inflammasome by Ozone Exposure. *Free Radic. Biol. Med.* 152, 561–570. doi:10.1016/j.freeradbiomed.2019.11.031

Ferrara, F., Pambianchi, E., Woodby, B., Messano, N., Therrien, J.-P., Pecorelli, A., et al. (2021). Evaluating the Effect of Ozone in UV Induced Skin Damage. *Toxicol. Lett.* 338, 40–50. doi:10.1016/j.toxlet.2020.11.023

Gao, Z., Zhao, D., Cheng, Q., Zhao, D., Yang, Y., Tian, Y., et al. (2021). Mesoporous SiO 2 -Encapsulated Nano-Co 3 O 4 Catalyst for Efficient CO Oxidation. *Chemcatchem* 13, 4010–4018. doi:10.1002/cctc.202100602

Gong, S., Chen, J., Wu, X., Han, N., and Chen, Y. (2018). *In-situ* Synthesis of Cu2O/reduced Graphene Oxide Composite as Effective Catalyst for Ozone Decomposition. *Catal. Commun.* 106, 25–29. doi:10.1016/j.catcom.2017.12.003

Gong, S., Li, W., Xie, Z., Ma, X., Liu, H., Han, N., et al. (2017). Low Temperature Decomposition of Ozone by Facilely Synthesized Cuprous Oxide Catalyst. *New J. Chem.* 41, 4828–4834. doi:10.1039/c7nj00253j

Gopi, T., Swetha, G., Chandra Shekar, S., Ramakrishna, C., Saini, B., Krishna, R., et al. (2017). Catalytic Decomposition of Ozone on Nanostructured Potassium and Proton Containing δ-MnO2 Catalysts. *Catal. Commun.* 92, 51–55. doi:10.1016/j.catcom.2017.01.002

Jia, J., Zhang, P., and Chen, L. (2016). Catalytic Decomposition of Gaseous Ozone over Manganese Dioxides with Different Crystal Structures. *Appl. Catal. B: Environ.* 189, 210–218. doi:10.1016/j.apcatb.2016.02.055

Khan, S. A., Khan, S. B., and Asiri, A. M. (2015). Core-shell Cobalt Oxide Mesoporous Silica Based Efficient Electro-Catalyst for Oxygen Evolution. *New J. Chem.* 39, 5561–5569. doi:10.1039/c5nj00521c

Kim, S. H., An, H.-R., Lee, M., Hong, Y., Shin, Y., Kim, H., et al. (2022). High Removal Efficiency of Industrial Toxic Compounds through Stable Catalytic Reactivity in Water Treatment System. *Chemosphere* 287, 132204. doi:10.1016/j.chemosphere.2021.132204

Li, X., Ma, J., and He, H. (2020). Recent Advances in Catalytic Decomposition of Ozone. *J. Environ. Sci.* 94, 14–31. doi:10.1016/j.jes.2020.03.058

Ma, J., Wang, C., and He, H. (2017). Transition Metal Doped Cryptomelane-type Manganese Oxide Catalysts for Ozone Decomposition. *Appl. Catal. B: Environ.* 201, 503–510. doi:10.1016/j.apcatb.2016.08.050

Namdari, M., Lee, C.-S., and Haghighat, F. (2021). Active Ozone Removal Technologies for A Safe Indoor Environment: A Comprehensive Review. *Building Environ.* 187, 107370. doi:10.1016/j.buildenv.2020.107370

Nazaroff, W. W., and Weschler, C. J. (2021). Indoor Ozone: Concentrations and Influencing Factors. *Indoor Air* 00, 1–21. doi:10.1111/ina.12942

Nikolov, P., Genov, K., Konova, P., Milenova, K., Batakliev, T., Georgiev, V., et al. (2010). Ozone Decomposition on Ag/SiO2 and Ag/clinoptilolite Catalysts at Ambient Temperature. *J. Hazard. Mater.* 184, 16–19. doi:10.1016/j.jhazmat.2010.07.056

Ou, J., Yuan, Z., Zheng, J., Huang, Z., Shao, M., Li, Z., et al. (2016). Ambient Ozone Control in a Photochemically Active Region: Short-Term Despiking or Long-Term Attainment? *Environ. Sci. Technol.* 50, 5720–5728. doi:10.1021/acs.est.6b00345

Tang, W.-X., Liu, H.-D., Wu, X.-F., and Chen, Y.-F. (2014a). Higher Oxidation State Responsible for Ozone Decomposition at Room Temperature over Manganese and Cobalt Oxides: Effect of Calcination Temperature. *Ozone: Sci. Eng.* 36, 502–512. doi:10.1080/01919512.2014.894454

Tao, Z., Fu, M., and Liu, Y. (2021b). A Mini-Review of Carbon-Resistant Anode Materials for Solid Oxide Fuel Cells. *Sust. Energ. Fuels* 5, 5420–5430. doi:10.1039/d1se01300a7

Tao, Z., Fu, M., Liu, Y., Gao, Y., Tong, H., Hu, W., et al. (2021a). High-performing Proton-Conducting Solid Oxide Fuel Cells with Triple-Conducting Cathode of Pr0.5Ba0.5(Co0.7Fe0.3)O3-δ Tailored with W. *Int. J. Hydrogen Energ.* doi:10.1016/j.ijhydene.2021.10.145

Xie, R., Li, D., Hou, B., Wang, J., Jia, L., and Sun, Y. (2011). Solvothermally Derived Co3O4@m-SiO2 Nanocomposites for Fischer-Tropsch Synthesis. *Catal. Commun.* 12, 380–383. doi:10.1016/j.catcom.2010.10.010

Yang, S., Zhu, Z., Wei, F., and Yang, X. (2017). Carbon Nanotubes/Activated Carbon Fiber Based Air Filter media for Simultaneous Removal of Particulate Matter and Ozone. *Building Environ.* 125, 60–66. doi:10.1016/j.buildenv.2017.08.040

Yu, Y., Ji, J., Li, K., Huang, H., Shrestha, R. P., Kim Oanh, N. T., et al. (2020). Activated Carbon Supported MnO Nanoparticles for Efficient Ozone Decomposition at Room Temperature. *Catal. Today* 355, 573–579. doi:10.1016/j.cattod.2019.05.063

Zhu, G., Zhu, W., Lou, Y., Ma, J., Yao, W., Zong, R., et al. (2021). Encapsulate α-MnO2 Nanofiber within Graphene Layer to Tune Surface Electronic Structure for Efficient Ozone Decomposition. *Nat. Commun.* 12, 10. doi:10.1038/s41467-021-24424-x

Conflict of Interest: The authors declare that the research was conducted in the absence of any commercial or financial relationships that could be construed as a potential conflict of interest.